

Hydrologic windows into the crystalline basement and their controls on groundwater flow patterns across the Paradox Basin, western USA

M. Person^{1,†}, J.C. McIntosh², J.-H. Kim^{2,3}, C. Noyes², L. Bailey⁴, S. Lingrey⁴, R. Krantz⁴, D. Lucero¹, P.W. Reiners⁴, and G. Ferguson^{5,2}

¹Hydrology Program, Department of Earth and Environmental Science, New Mexico Tech, 801 Leroy Place, Socorro, New Mexico 87801, USA

ABSTRACT

Conceptual models of sedimentary basin groundwater flow systems typically assume that the crystalline basement acts as an impermeable boundary and can be neglected. In this study, we use hydrologic models constrained by isotopic and geochemical datasets to argue that the La Sal Mountains, Utah, USA, act as a hydrologic window into the Paradox Basin's lower aquifer system and underlying crystalline basement. We conducted a sensitivity study in which we varied crystalline basement/laccolith permeability as well as fault zone connectivity along a cross-sectional transect from the La Sal Mountains to Lisbon Valley. When the crystalline basement/laccolith units are set at relatively permeable levels (10⁻¹⁴ m²), simulated tracers that include total dissolved solids, oxygen isotopic composition of pore fluids (δ^{18} O), and groundwater residence times are in closest agreement with field measurements. Model results indicate that pore fluids in the basal aquifer system underlying the Paradox Formation confining unit are a mixture of relatively young meteoric fluids and older Paradox Formation brines. The presence of faults did not significantly modify fluid exchange between the upper and lower aquifer systems. This was due, in part, to underpressuring within the Paradox Formation. Our study concludes that the Paradox Basin represents a regional recharge area for

M.Person https://orcid.org/0000-0003-0503-1845 mark.person@nmt.edu

the Colorado Plateau, with groundwater discharge occurring along the Colorado River within the Grand Canyon some 375 km away to the southwest. This is only possible with a permeable crystalline basement. Our findings help explain the genesis of Mississippi Valley-type ore deposits of the US Midcontinent, where the presence of a permeable basement may be useful in addressing issues related to solute mass and energy balance.

INTRODUCTION

Hydrogeologists typically neglect the crystalline basement when developing conceptual and quantitative models of regional groundwater flow systems (Taucare et al., 2020; Meyers et al., 2021). The permeability of siliciclastic and carbonate rocks is typically assumed to be orders of magnitude higher than that of fractured crystalline basement rocks. However, convective heat-flow anomaly data and inferences of solute mass transport gleaned from metamorphic systems suggest that the crystalline basement is permeable to depths of 10 km (Manning and Ingebritsen, 1999; Ingebritsen and Manning, 2010). Fluid residence times, constrained by noble gases, show enhanced permeability within the upper 1 km of Precambrian basement rocks (Ferguson et al., 2023). Continental-scale compilations of pore-fluid stable isotopic data show deeper meteoric water circulation (up to \sim 5 km depth) in areas of relatively high topographic relief (McIntosh and Ferguson, 2021). Tertiary-age, δ18O-depleted plutonic rocks in western North America presented by Gregory et al. (1989) argue for meteoric fluid circulation

to depths of $\sim \! 10$ km. Deep circulation within the crystalline basement has also been shown to have important implications for mountain-front recharge (Frisbee et al., 2017), deep subsurface microbial activity (Lollar et al., 2019), and near-surface ecosystem health. Deep circulation systems are a global phenomenon (e.g., Stober, 1996; Stober and Bucher, 2004, 2007, 2015a; Bucher et al., 2009; Stober et al., 1999; Bucher et al., 2009; Stober et al., 2016) and explain most thermal anomalies, mineralized springs, and changes in regional hydrochemistry of aquifer systems in contact with basement rocks.

This study focuses on understanding groundwater flow interactions between the crystalline basement and sedimentary units of the Paradox Basin, Utah, USA. The Paradox Basin hydrogeologic system is conceptualized as having an upper and lower aquifer system separated by the Paradox Formation confining unit (Fig. 1C; Thackston et al., 1981). The upper aguifer system includes the Navajo Sandstone, Burro Canyon, Cutler, and Honaker Trail formations. The Redwall Limestone is the principle aquifer of the lower aquifer systems. The Paradox Formation, comprised of evaporites and organic-rich shales (Nuccio and Condon, 1996), acts as a tight confining unit that separates the two aquifer systems. In some regions across the Colorado Plateau, the Paradox Formation acts as a seal, trapping CO₂ and He within underlying reservoir rocks (Heath et al., 2017; Tyne et al., 2022). Across the Paradox Basin, faults act as conduits for hydrocarbons and CO₂ (Shipton et al., 2004), and in the geologic past, also for ore-forming fluids (Jacobs and Kerr, 1965; Chan et al., 2000; Chan et al., 2001; Bailey et al., 2022). Faults are

https://doi.org/10.1130/B37063.1.

GSA Bulletin; published online 12 January 2024

> © 2024 The Authors. Gold Open Access: This paper is published under the terms of the CC-BY license.

²Department of Hydrology and Atmospheric Sciences, The University of Arizona, 1133 East James E. Rogers Way, Tucson, Arizona 85721, USA

³Korea Institute of Geoscience and Mineral Resources, Daejeon, 34132, Republic of Korea

⁴Department of Geosciences, The University of Arizona, 1040 East Fourth Street, Tucson, Arizona 85721, USA

⁵Department of Civil, Geological and Environmental Engineering, University of Saskatchewan, 57 Campus Drive, Saskatoon, Saskatchewan S7N 5A9, Canada

also associated with modern springs (Thackston et al., 1981).

What is perhaps less appreciated is the role of relatively permeable crystalline basement rocks in controlling recharge and deep regional groundwater flow patterns across the Paradox Basin. Geochemical, isotopic, and noble gas data presented by Kim et al. (2022a) and Tyne et al. (2022) indicate that meteoric fluids mixed with Paradox Formation brines within the Red-

wall Limestone and McCracken Sandstone. This could only be accomplished if the La Sal Mountains were acting as a recharge tower for the lower aquifer system. Here, we define the crystalline basement as including both Precambrian igneous/metamorphic and 28 Ma laccolith units (Condon, 1997). Triggered seismicity related to saline brine injection within the crystalline basement 1.2 km beneath the Redwall Limestone (Ake et al., 2005) suggests that the

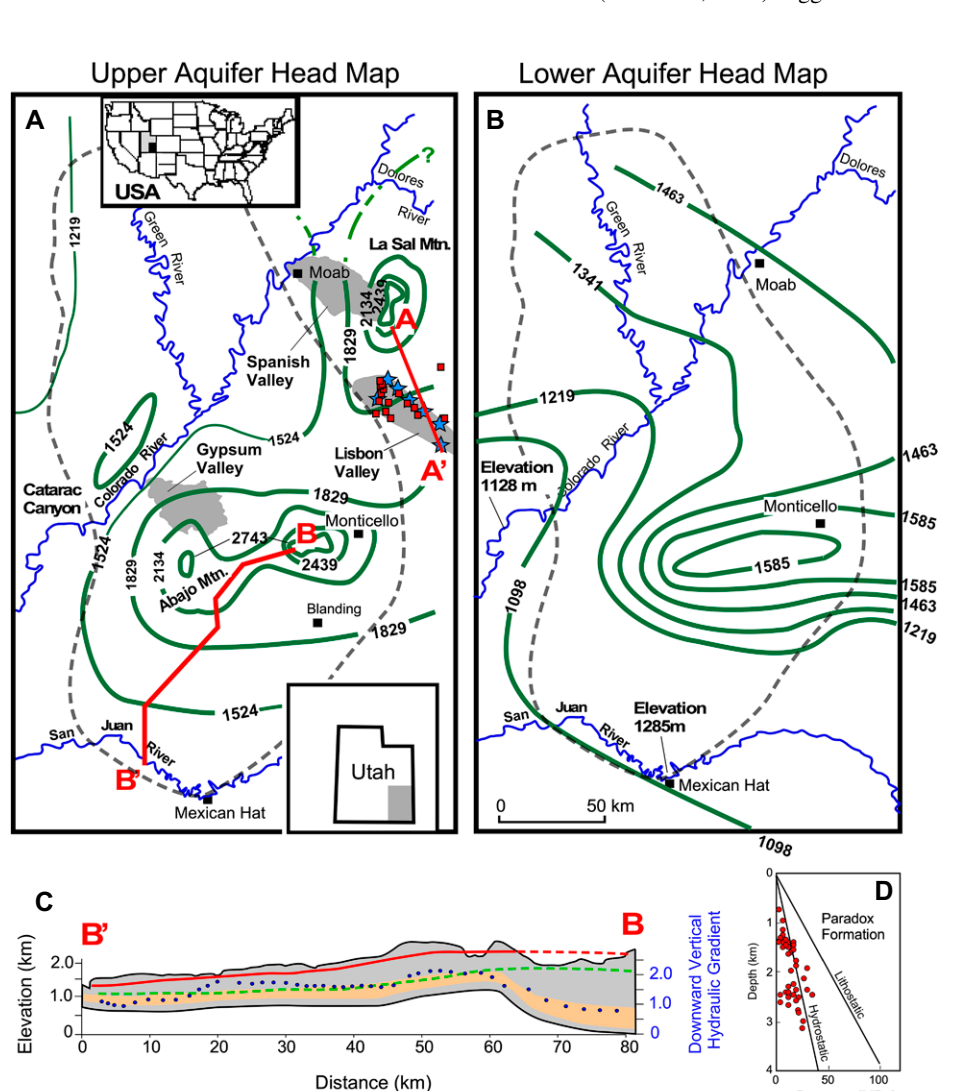


Figure 1. Hydraulic head maps for (A) upper and (B) lower aquifer systems (after Thackston et al., 1981). In panel A, blue stars and red squares denote the locations of wells where geochemical samples and temperatures were collected (see Fig. 7D) within Lisbon Valley (gray shaded pattern). Two insets in panel A show the location of the study area in the USA and the state of Utah. Red line A–A′ depicts the approximate location of the cross-sectional models described below. Red line B–B′ denotes the location of the cross section in panel C. (C) Upper and lower aquifer system potentiometric surfaces are denoted by the red and green lines along B–B′, respectively. Blue dots denote the downward hydraulic gradient between the upper and lower aquifer systems. Orange pattern depicts the position and thickness of the Paradox Formation separating the upper and lower aquifer systems. (D) Paradox Formation pressure data from shut-in test data within the Paradox Basin Formation are from Allis (2013).

crystalline basement has non-negligible permeability (Zhang et al., 2013). The injection rates reported by Ake et al. (2005) are too high to be accommodated by low-permeability basement rocks. Crystalline basement-hosted springs discharging along the Colorado River in the Grand Canyon are additional evidence for a permeable crust (Crossey et al., 2009). In this study, we hypothesize that where the crystalline basement outcrops, such as within the La Sal and Abajo Mountains (Fig. 1A), it acts as a hydrologic window, permitting meteoric fluids to descend beneath the Paradox Formation confining unit and recharge the lower aquifer system. The concept of hydrologic windows was first proposed to explain the locations of groundwater up-flow zones associated with crystalline basementhosted hot springs along the Rio Grand Rift in New Mexico (Barroll and Reiter, 1990; Mailloux et al., 1999; Pepin et al., 2012). However, we argue below that this conceptual model equally applies to groundwater recharge areas.

To assess groundwater flow interactions between the crystalline basement and overlying/ adjacent sedimentary units within the Paradox Basin, we constructed a suite of cross-sectional paleo-hydrogeologic models. The models solve for variable-density groundwater flow, heat, and solute transport. We also tracked advective-dispersive isotopic (δ¹⁸O) transport and groundwater residence times (Goode, 1996). Because we compared our model results to geochemical and isotopic data presented by Kim et al. (2022a), our study is focused on the Pleistocene to Modern groundwater flow system originating within the La Sal Mountains and flowing southeast across Lisbon Valley, Utah. We allowed water-table elevations and the oxygen isotopic composition of recharge within the La Sal Mountains to vary between glacial cycles over a 1 m.y. period in an attempt to replicate Pleistocene climate forcing.

We addressed the following questions: How permeable is the crystalline basement within the Paradox Basin? To what extent does the crystalline basement modify the transport of geochemical tracers within the lower aquifer system? How do faults and fault-zone connectivity influence groundwater flow patterns? Have the groundwater flow system and geochemical/isotopic tracers within the Paradox Basin arrived at a dynamic equilibrium with the modern climate?

GEOLOGIC SETTING

The sedimentary units of the Paradox Basin discussed in this study are listed in Table 1. Prior to formation of the Paradox Basin during Cambrian and Devonian times, marine shales, sandstones, and carbonates were deposited, including the McCracken Sandstone and the Ouray Lime-

TABLE 1. LITHOLOGIC DESCRIPTION, PERMEABILITY, POROSITY, AND ROCK THERMAL CONDUCTIVITY USED IN THE LISBON VALLEY PALEOHYDROLOGIC MODELS

Log ₁₀ [k _x]	Log ₁₀ [k _z]	ф	(W/[m °C])	Formation and description	Color
-18	-19	0.2	2.5	Mancos Shale: fossiliferous shale with some limestone in concretions.*	Yellow
-13.3	-15.3	0.2	2.5	Burro Canyon Formation: conglomerate, medium- to fine-grained sandstone.†	Dark olive
-17	-19	0.05	2.5	Morrison Formation: interbedded sandstone, siltstone, and shale layers; confining unit.§	Light green
-13.3	-15.3	0.1	2.5	Navajo/Glenn Canyon Group: massive eolian, sandstone.*	Dark green
-14	-17	0.05	2.5	Chinlee/Moenkopi: sandstone, siltstone, and shale.§	Aguamarine
-14.7	-17	0.1	2.5	Cutler Formation: well-bedded, hematite-stained sandstone.*	Blue-green
-13	-15	0.1	2.5	Honaker Trail Formation: alluvial-fan, fluvial, flood-plain, playa, eolian, and tidal-flat.§	Light blue-green
-20	-20	0.01	5.0	Paradox Formation: gypsum, anhydrite, and salt, interbedded with shale, sandstone, and limestone.#	Dark blue
-13	-14	0.1	2.5	Lower aguifer system: includes the Redwall Limestone and McCracken formations.**	Blue
-14	-14	0.05	2.5	Crystalline basement: granite, granitic gneiss, hornblende schist cut by pegmatite veins.*	Purple
-16	-16				•
-18	-18				
-14	-14	0.05	2.5	La Sal Laccolith: diorite and monzonite porphyry with sills and dikes.*	Dark purple
-16	-16	0.00	0	La da. Laccomin de la monte de perpriy, y min dina dina dinad	Dain parpio
-18	-18				
-16 -16	-16 -14	0.2	2.5	Faults assigned conduit-barrier properties. Faults cut the Paradox Formation, terminating at the base	Sub-vertical red
-10	-14	0.2	2.5	of the model domain.	lines

Note: See Figure 2 to relate colors to hydrostratigraphic unit properties.

stone, in a continental platform environment (Condon, 1997). The Ordovician and Silurian eras were a period of nondeposition (Condon, 1997). During the Mississippian, a marine transgression resulted in deposition of the Redwall Limestone. Paradox Basin deposition began in earnest during Pennsylvanian-Permian times with the ancestral Rocky Mountains and Uncompangre uplift. During the Pennsylvanian, the Paradox Formation was deposited to the west of the Uncompangre uplift. Organic-rich shale, dolomite, and evaporite units were deposited in a marginal marine environment during cycles of marine flooding and regression. Goldhammer et al. (1991) defined 34 Milankovich-driven carbonate cycles during the middle Pennsylvanian. Ductile deformation of the salt beds occurred as sediment was shed off the Uncompangre uplift (Barbeau, 2003) to create the Honaker Trail and Cutler formations. Salt tectonics led to the development of a series of mini-basins (Rasmussen and Rasmussen, 2009), including Lisbon Valley. This was followed by the deposition of continental units, including the Mesa Verde Group, which includes the aeolian Navajo Sandstone and the Morrison and Burro Canyon formations. During the Cretaceous, western North America was inundated by a shallow sea, which resulted in the deposition of the Mancos Shale. Up to 2 km of marine shales were deposited across the Colorado Plateau during the Cretaceous. The Cenozoic was a period of relative stability and nondeposition (Murray et al., 2016). During the Oligocene, a series of laccoliths were emplaced across the Colorado Plateau, including the La Sal complex (Hunt and Waters, 1958). Rapid erosion over the past 2-5 m.y. (Murray et al., 2016) associated with downcutting of the Colorado River

and its tributaries, including the Dolores River, resulted in the formation of the La Sal Mountains, which initiated a regional, topographically driven groundwater flow system.

Climate

In La Sal, Utah (elevation 2127 m), a community on the southern side of the La Sal Mountains close to Lisbon Valley, the mean annual temperature is 8.4 °C, and the precipitation is 487 mm (Noyes et al., 2021). Modern evapotranspiration rates exceed precipitation within the lowlands (Table S11). Annual precipitation within the La Sal Mountains (elevation 3880 m) is up to 0.83 m (Richmond, 1972). Present-day and paleo-recharge rates were estimated in this study using monthly temperature and precipitation data described in the Supplemental Material. In the desert southwest during the Last Glacial Maximum (LGM), temperatures are estimated to have been at least 5-7 °C cooler, and precipitation is thought to have doubled in New Mexico, USA, which led to the formation of a number of Pleistocene lakes (Benson, 1988; Phillips et al., 1986; Menking et al., 2004; Allen, 2005; Asermon et al., 2010; Reheis et al., 2014). We hypothesize that isotopic/chemical tracers were modified by Pleistocene climatic cycles. Table S1 estimates how temperature, evapotranspiration, recharge, and the stable oxygen isotopic composition of water (δ^{18} O) in

¹Supplemental Material. Supplemental materials discuss the transport equations used in the manuscript. Please visit https://doi.org/10.1130 /GSAB.S.24512821 to access the supplemental material, and contact editing@geosociety.org with any questions.

precipitation may have varied between modern times and the LGM. Figure S1 plots changes in simulated isotopic composition at the land surface within the La Sal Mountains and beneath Lisbon Valley during the Pleistocene. Some prior studies indicated that recharge may have been up to three times greater than Holocene levels during the LGM (Zhu et al., 2003). It is likely that some of this available excess water increased runoff during periods of glaciation (Putnam and Broecker, 2017) more than diffuse recharge. In this study, we assume that LGM temperature reduction resulted in ¹⁸O-depleted recharge (Noyes et al., 2021).

Hydrogeology

Hanshaw and Hill (1969) presented hydrologic and geochemical analyses of the Paradox Formation, Redwall Limestone, and Cutler and Honaker Trail formations (Fig. 2A). They found that, with few exceptions, the salinity (i.e., total dissolved solids) of formation waters in the upper aquifer units ranged from fresh (<1 ppt) to brackish (<10 ppt). However, the Paradox Formation contained brines with up to 400 ppt of salinity. As noted above, Thackston et al. (1981) conceptualized Paradox Basin hydrogeology as having upper and lower aquifer systems separated by the Paradox Formation (evaporites), which serves as the regional confining unit (orange pattern, Fig. 1C). Analysis of head maps (Figs. 1A and 1B) indicates a consistently downward vertical head gradient (blue circles, Fig. 1C). Drill-stem test data (Allis, 2013) reveal fluid underpressure levels of up to 20 MPa (2000 m) within the Paradox Formation (Fig. 1D). This is likely due, in part,

^{*}Hunt and Waters (1958)

[†]Simmons (1957)

[§]Cole et al. (1996)

[#]Baker et al. (1933)

^{**}McKee and Gutschick (1969)

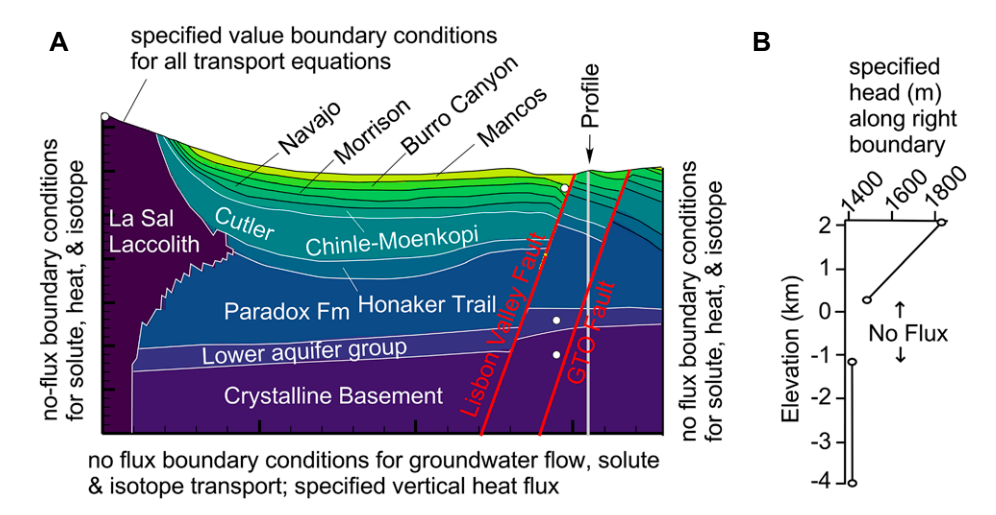


Figure 2. (A) Hydrostratigraphy and imposed boundary conditions for present-day Lisbon Valley model. Solid red lines denote the vertical extent of the fault zones that extend to the bottom of the model domain. White dots indicate the locations of monitoring points of the time series plot presented in Figure 3. Values of aquifer parameters are listed in Tables 1, 3, and 4. Lower aquifer group includes the Redwall Limestone and the McCracken Formations. (B) Specified head and no-flow boundary conditions imposed along southern edge of model domain.

to rapid uplift and erosion (Corbet and Bethke, 1992) that began \sim 2–5 m.y. ago (Murray et al., 2016) or possibly dehydration reactions (Stober and Bucher, 2004). Underpressures within the upper and lower aquifer systems are also likely due to the effects of topography-driven flow (Belitz and Bredehoeft, 1988). Plan-view contour maps of upper (Fig. 1A) and lower (Fig. 1B) piezometric surfaces indicate that the La Sal and Abajo mountains (laccolith intrusions) are acting as recharge towers related to orographic precipitation effects. The lack of upward vertical head gradients in topographically low-lying regions suggests that much of the Paradox Basin acts as a recharge area for the greater Colorado Plateau.

Reitman et al. (2014) developed a threedimensional model of variable-density groundwater flow and solute transport to quantify salt loading into the Colorado River within Gypsum Valley, which is located ~ 100 km to the southwest of Lisbon Valley and receives recharge from the Abajo Mountains. They performed a model calibration exercise using water levels and salinity data and estimated that the annual mass of salt dissolved within the upper aguifer system contributed $\sim 2.2 \times 10^5$ kg to the Colorado River in Gypsum Valley. Gardner et al. (2020) used a suite of geochemical and isotopic tracers to estimate the location and magnitude of recharge from the La Sal Mountains to Spanish Valley, which is near Moab (Fig. 1A). The principle aquifer in their study area is the Glenn Canyon Group, which includes the Navajo Sandstone. Groundwater flow was from the La Sal Mountains, with discharge into the Colorado River in low-lying areas near Moab, Utah. These authors concluded that there is little depression-focused recharge along arroyos, with the bulk of the recharge occurring at high elevations within the La Sal Mountains. Because the Glenn Canyon Group does not crop out in the uplands, they concluded that much of the recharge is provided via the crystalline basement. Their estimated recharge rate, using a lumped-parameter model, was ~0.09 m/yr. Corrected ¹⁴C ages for the Glenn Canyon Group aquifer ranged between 1700 years and 3700 years, with a mean residence time of 2700 years.

Noyes et al. (2021) used water-well levels and isotopic tracer data to assess the hydrologic connection between the Burro Canyon and Navajo

aguifers within Lisbon Valley. Water-level data indicated a relatively high vertical hydraulic gradient (~6.7) between the Navajo and Burrow Canyon aquifers, which are separated by the Morrison Formation. This hydraulic gradient is three times what is reported in Figure 1C. Stable isotopic compositions of water ($\delta^{18}O$ and $\delta^{2}H$) and ¹⁴C ages in these two aquifers are distinctive. The Burro Canyon pore fluids are Holocene in age (11-3.3 ka), while fluids within the Navajo Sandstone are late Pleistocene in age (36–15 ka). Scatter plots of δ¹⁸O, δ²H, and ¹⁴C data indicated that the older groundwater within the Navajo aquifer is isotopically depleted, which is consistent with recharge under cooler conditions during the late Pleistocene. The Navajo aquifer crops out at a higher elevation in the foothills of the La Sal Mountains, which could also partially explain the more depleted isotopic composition. Noves et al. (2021) concluded that there was little hydrologic communication between the Burro Canyon and Navajo aquifers.

Permeability data for different formations within the Paradox Basin can be found in Woodward-Clyde Consultants (1982), Freethey and Cordy (1991), and Lopes and Hoffmann (1997). We summarize the data in Table 2. For the Paradox Formation evaporites, we relied on measurements from field-pressure tests carried out in situ in bedded salt at the medium-level nuclear waste repository near Carlsbad, New Mexico, as reported in Beauheim and Roberts (2002). For Mancos Shale permeability, we relied on laboratory core measurements reported in Gutierrez et al. (2015). It is worth noting that core measurements can underestimate permeability (Stober and Bucher, 2015a). Neuzil (1994) pointed out that lab measurements were 10^{-20} m^2 compared to the $10^{-16} \ m^2$ Bredehoeft et al. (1983) estimated at the regional scale. Porosity data for the Paradox Basin sedimentary units varied between ~ 0.05 and 0.2 (Cappa and Rice, 1995; Chidsey et al., 2003; Woodward-Clyde Consultants, 1982; Clem and Brown, 1984). We

TABLE 2. PARADOX BASIN PERMEABILITY DATA (m2)

Avg.	Max.	Min.	N	
-17.7	-15.7	-19.7	2	
-12.9	-12.7	-13.4	39	
-13.5	-13.4	-13.7	43	
-14.3			1	
-12.6	-12.1	-13.8	42	
-16.3			1	
-13.6	-13.3	-15.0	8	
-14.3	-14.0	-15.2	2	
-14.0	-13.3	-19.0	30	
-14.1	-12.7	-19.0	84	
-19	-18	-23	30	
-13.2	-11.8	-16.7	63	
-15.0	-14.1	-17.4	15	
	-17.7 -12.9 -13.5 -14.3 -12.6 -16.3 -13.6 -14.3 -14.0 -14.1 -19 -13.2	-17.7 -15.7 -12.9 -12.7 -13.5 -13.4 -14.3 -12.6 -12.1 -16.3 -13.6 -13.3 -14.3 -14.0 -13.3 -14.1 -12.7 -19 -18 -13.2 -11.8	-17.7	

Note: Avg.—average; Max.—maximum; Min.—minimum; N.—number of observations. Sources: Woodward-Clyde Consultants (1982), Freethey and Cordy (1991), Kirby (2008), Lopes and Hoffmann (1997), and Gutierrez et al. (2015).

*Beauheim and Roberts (2002)

assigned a relatively high value of porosity for the crystalline basement rocks (0.05; Table 1). However, similar porosity values (0.023) have been inferred from tracer tests within the crystalline basement along the Rhine Graben at depths of 2–4 km (Aquilina et al., 2004).

METHODS

We constructed NW-SE cross-sectional hydrothermal models (FEMOC; Person et al., 2007) from the La Sal Mountains across Lisbon Valley (red line A-A' in Fig. 1A). The model domain has a maximum thickness of 7.3 km and is 36 km in lateral extent (Fig. 2A). We included \sim 2 km of crystalline basement beneath the basal aquifer group. The upper aquifer system includes the Honaker Trail, Cutler, Navajo Sandstone, and Burro Canyon formations. These aquifer units are separated by confining units that include the Chinle-Moenkopi formations, Morrison Formation, and Mancos Shale. The Mancos Shale is absent in portions of Lisbon Valley. The lower aguifer system includes the McCracken Sandstone and Redwall Limestone. These two units were lumped into a single unit in our model. Also included in our model are the La Sal Laccolith and underlying granitic/metamorphic basement rocks (Condon, 1997). We included two fault zones in our study. The crystalline basement varied between 10^{-16} m² and 10^{-14} m² in the two fault scenarios. The faults were assigned fault permeabilities two orders of magnitude higher in the z-direction (10^{-14} m^2) than in the x-direction (10^{-16} m²). These subvertical faults extend through the Paradox Formation to the base of the model domain (solid red lines in Fig. 2A). The GTO and Lisbon Valley fault zone elements have widths of 98 m and 133 m, respectively. The model is comprised of 2846 nodes and 5466 triangular elements. Near the La Sal Mountains, elements have a maximum width of \sim 770 m. Vertical discretization varied between ∼110 m (sedimentary units) and 760 m (crystalline basement elements). We considered additional fault scenarios (not shown) where the faults terminated within the Paradox Formation. We found that they had little effect on the salinity within the crystalline basement.

We solved a variable-density groundwater flow equation (Equation A1 in the Supplemental Material). The dependent variable is the equivalent freshwater head (Fig. 3). We included a sink term in the groundwater flow equation to approximate the development of underpressure due to erosional unloading (Corbet and Bethke, 1992). We did not remove sediments (nodes) along the top surface of the model domain during the 1 m.y. simulation period; for the fluid sink term, we assumed an erosion rate of

TABLE 3. PARAMETERS THAT WERE NOT VARIED IN THE SENSITIVITY STUDY

Parameter	Value	Comment
S _s	3 × 10 ⁻⁵ m ⁻¹	Specific storage
∂L/∂t	0.4 mm yr ⁻¹	Erosion rate
α_{L}	10 m	Longitudinal dispersivity
α_{L}	1 m	Transverse dispersivity
D_d	10 ⁻¹⁰ m/s ²	Solute diffusivity
λ_{f}	0.58 W/(m °C)	Water thermal conductivity
c_s	790 J/(kg °C)	Specific heat
C _f	4184 J/(kg °C)	capacity of rock Specific heat capacity of water

0.4 mm/yr, which is consistent with the removal of 2 km of Mancos Shale over a period of 5 m.y. (Table 3). We assigned a relatively high specific storage coefficient of 3×10^{-5} m⁻¹ to accentuate the development of underpressure within the Paradox Formation (Fig. 1D). This high specific storage coefficient had relatively little effect on computed transient heads within aquifer units.

Equivalent freshwater heads become high if brines are present, but they cannot be used to directly infer directions of vertical groundwater flow because of buoyancy effects (Post et al., 2007). We solved a conductive-convective heat transport equation as well as a series of advective-dispersive transport equations, including transport of solute, isotopic tracers (δ¹8O), and mean groundwater residence times (Equations A3–A8 in the Supplemental Material). We neglected fluid-rock isotope exchange reactions due to the relatively shallow depth and associ-

ated low temperatures ($<160\,^{\circ}$ C). The equations were solved using the finite element method. We used the modified method of characteristics to approximate advective transport.

We imposed specified-value boundary conditions along the top boundary for heat, solute, and isotopic transport, along with groundwater residence time (Fig. 2A). The bottom boundary conditions were all no flux except for heat transport (Fig. 2A). We used a specified heat flux of 60 mW/m² along the bottom of the model domain. Within the La Sal Mountains, we allowed specified heads to fluctuate by up to 20 m during glacial-interglacial periods of the Pleistocene (Paces et al., 2020). This resulted in only a small increase in recharge, far less than that reported by Zhu et al. (2003). We applied a specified head along the southern edge of our model domain to allow fluids to exit Lisbon Valley (Figs. 2B and 3). Heads decreased from 1830 m to 1400 m between the top and base of the model domain except along the Paradox Formation (Fig. 2B). The imposed decrease in head with depth is consistent with the potentiometric maps of Thackston et al. (1981). By not imposing a specified head along the Paradox Formation, we allowed underpressures to develop within the Paradox Formation that were not influenced by this boundary. A spring boundary (also known as a no-diffusive-flux boundary) was imposed for the other transport equations along this edge. No-flux boundaries were imposed along the northern edge of the model domain.

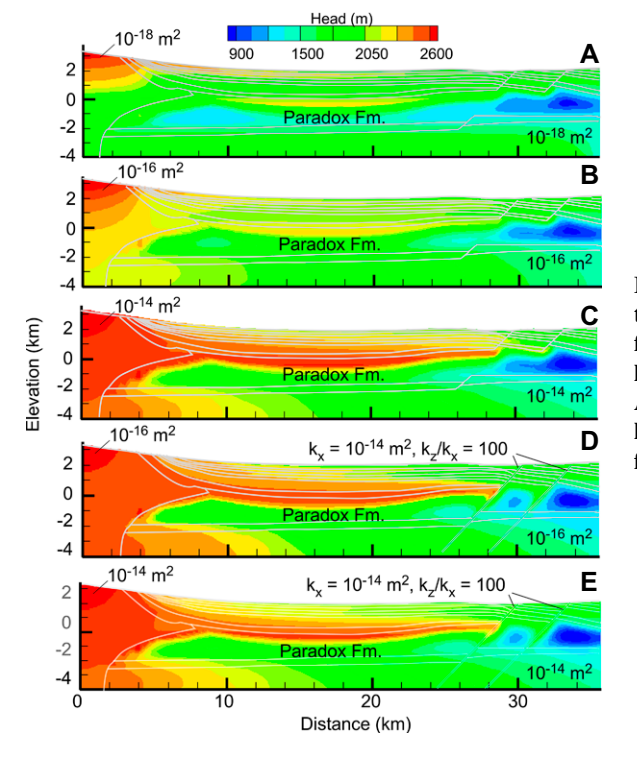


Figure 3. Computed heads for the present-day Lisbon Valley flow system. See Figure 1A for location of cross-section line A-A'. The translucent white lines denote formation and fault boundaries.

We assumed local hydrostatic initial conditions for groundwater flow, and imposed a linear increase in salinity, temperature, and mean groundwater residence time with depth. Initial salinity conditions increased with depth from 0 ppt at the land surface to 300 ppt at the base of the model domain. Initial pore fluid residence time increased linearly from 0 m.y. to 4 m.y. between the top and base of the model domain. Initial δ^{18} O varied from between about -13%to -17% at the land surface (Table S1) to about +9.3% at the base of the model domain. Within the Paradox Formation, we fixed salinity and δ^{18} O values to be equal to 300 ppt and 5%, respectively, during the simulation. Initial temperatures increased linearly using a subsurface geothermal gradient of 30 °C/km. We used computed initial conductive temperatures and equilibrium fractionation factors for a mineral assemblage that included quartz, anorthite, muscovite, biotite, hornblende, and calcite to set the initial δ^{18} O values of the fluids (Bowman et al., 1994). In our model, the modern mean annual land surface temperatures varied with elevation between 11.5 °C and 1.0 °C, given the change of 2100 m in elevation between the Lisbon Valley and the La Sal Mountains. During glacial times, δ18O values were decreased by 6% due to a 6 °C temperature reduction along the top boundary (water table). All simulations were initialized (spun up) and run for 1 m.y. to ensure that the initial salinity, residence times, and initial oxygen isotopic conditions would not have a significant impact on present-day model results. The models were then run at 1.05 m.y. using a time step size of 100 yr; solute and isotopic tracers have established dynamic equilibrium conditions by the end of the simulation. Model runs required up to two weeks of simulation time on our Linux cluster depending on the permeability level of the crystalline basement that was assigned.

We previously ran a number of simulations, varying the permeabilities of the upper and lower aquifer and confining unit. Some of these results can be found in Noyes (2019). In this study, we did not vary the permeability of the aguifer and confining units. Rather, our analysis focused on the effects of crystalline basement permeability and the presence or absence of faults on groundwater flow between the La Sal Mountains and Lisbon Valley. Based on ⁸¹Kr and δ¹⁸O measurements reported by Kim et al. (2022b), relatively young (ca. 1 Ma) meteoric fluids occur within the basal aquifer group. Noble gas results show extensive flushing of remnant basinal brines by meteoric recharge (Tyne et al., 2022). This would only be possible if the La Sal Laccoliths were sufficiently permeable to permit significant volumes of meteoric water to percolate down

TABLE 4. DESCRIPTION OF MODEL SCENARIOS

Scenario	Basement permeability (m²)	Fault present	Comment
1	10 ⁻¹⁸	No	Low crystalline basement permeability
2	10 ⁻¹⁶	No	Intermediate crystalline basement permeability
3	10 ⁻¹⁴	No	High crystalline basement permeability
4	10 ⁻¹⁶	Yes	Intermediate crystalline basement permeability
5	10 ⁻¹⁴	Yes	High crystalline basement permeability

and mix with basin brines beneath the Paradox Formation.

We used ⁸¹Kr and ¹⁴C age tracers, salinity, and δ¹⁸O data reported by Noyes et al. (2021) and Kim et al. (2022a, 2022b) to constrain and test our model results. Permeability and porosity values assigned to each of the 15 hydrostratigraphic units are presented in Table 1. The thermal conductivity of the Paradox Formation was set about twice as high as that of the clastic and carbonate units. Modeled scenarios and parameters considered in our sensitivity study are listed in Table 4.

RESULTS

Figure 3 presents contour maps of freshwater heads computed for the five scenarios considered in our sensitivity study (Table 4). Due to erosional unloading (0.4 mm/yr), the Paradox Formation had heads below hydrostatic conditions (up to ~970 m below hydrostatic conditions, or ~ 10 MPa in all modeled scenarios). Topography-driven flow dominates within the upper aquifer system. The northwest to southeast trend of increased hydraulic heads within the crystalline basement beneath the Paradox Formation is due to the increasing permeability of the La Sal Laccolith. As the permeability of the crystalline basement increased from 10⁻¹⁸ m² to 10⁻¹⁴ m² (Figs. 3A-3C), elevated heads propagated southward along the bottom 2 km of the model domain beneath the lower aquifer system. Because of the specified head boundary condition along the right (southern) edge of the model domain (Fig. 1B), groundwater migrated out of Lisbon Valley. Had we chosen a no-flow boundary for the entire right edge of the model domain, Lisbon Valley would have become a groundwater discharge area with upward hydraulic head gradients, which is inconsistent with the water-level measurements of Thackston et al. (1981) and Noyes et al. (2021). The presence of faults that cut the Paradox Formation in scenarios 4 and 5 allowed groundwater from the upper aquifer system to migrate down into the Paradox Formation, creating underpressured cells (Figs. 3D and 3E). Figure 4A presents vertical changes in hydraulic head beneath Lisbon Valley at x = 31 km; (vertical gray line in Fig. 2A indicates location of profile). Within the upper and lower aquifer systems, heads computed for all scenarios compare reasonably well to the estimated range of water levels within Lisbon Valley from the piezometric contour maps (Figs. 1A and 1B) of Thackston et al. (1981; see horizontal black lines in Fig. 4A). Computed heads within the upper aquifer system only agree with the shallowest portion of the hydraulic head data reported in Noyes et al. (2021). Note that only scenario 5 (green dashed line; crystalline basement permeability of 10^{-14} m²) produced a downward hydraulic gradient near the land surface that is consistent with field observations.

Flow rates and directions were sensitive to crystalline basement permeability (Fig. 5). A relatively small volume of deep recharge from the La Sal Mountains was focused into the lower aguifer system when the crystalline basement permeability was relatively low (10⁻¹⁸ m²; Figs. 4B and 5A); groundwater velocities (Darcy flux $[\vec{q}]$ divided by porosity $[\phi]$) within the lower aquifer system were only ~0.0028 m/yr for the low-permeability scenario (Fig. 4B), and 0.0005 m/yr within the underlying tight crystalline basement. Recharge into the upper aquifer system was controlled by the elevation where clastic units such as the Navajo Sandstone outcropped. When the permeability of the crystalline basement was raised to 10^{-16} m² or 10^{-14} m² (Table 4, scenarios 2 and 3; Figs. 5B and 5C), the flow rates in the lower aquifer system increased to \sim 0.1 m/yr (Fig. 4B), as this unit received significant recharge from the La Sal Mountains. When the crystalline basement was assigned a permeability of 10^{-16} m² or 10^{-14} m², recharge to the units of the upper aquifer system came not only from the La Sal Mountains across the water table but also from lateral flow below the land surface (Figs. 5B and 5C). The vertical velocity at the water table (top surface) within the La Sal Mountains for the high-permeability scenario was 4 m/ yr. Multiplying this by porosity (0.05) yields an estimated diffuse recharge rate (q_z) of 0.19 m/yr. Gardner et al. (2020) estimated a recharge rate of 0.09 m/yr based on lumped-parameter modeling and ¹⁴C groundwater ages. For the intermediate permeability scenario (10⁻¹⁶ m²), the vertical velocity of groundwater within the La Sal Mountains decreased to \sim 0.12 m/yr, lowering recharge to 0.006 m/yr, which is low in comparison to the rate of Gardner et al. (2020). Groundwater velocities within the crystalline basement increased from \sim 0.0002 m/yr to 0.05 m/yr to 4 m/yr as the crystalline basement permeability increased from

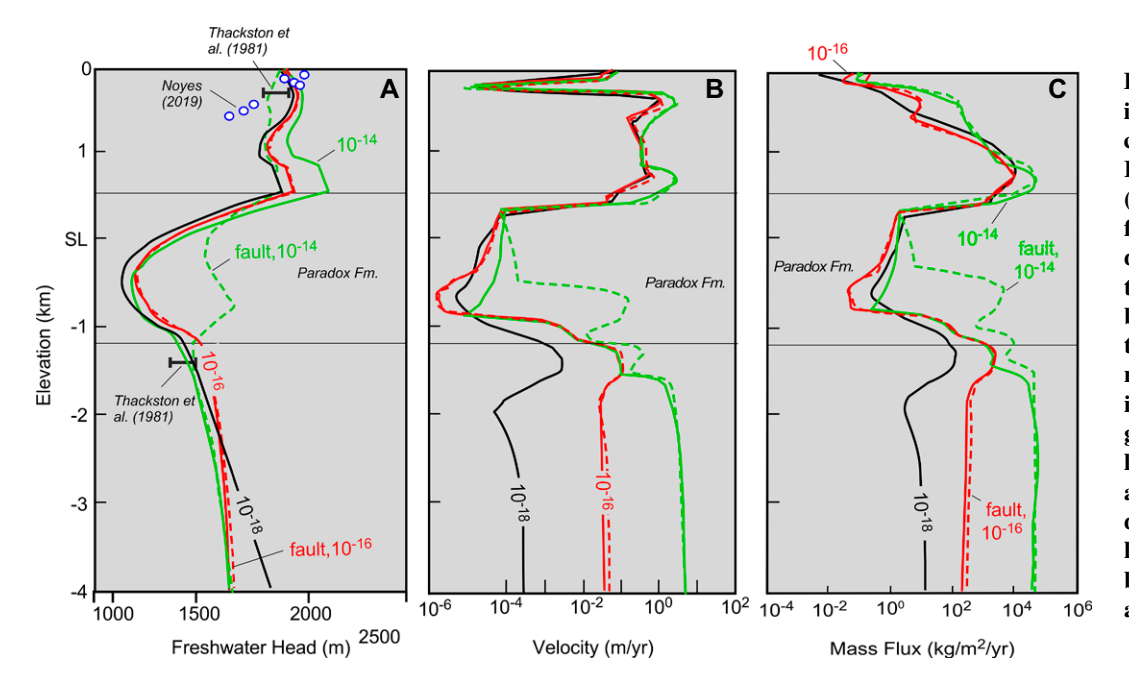


Figure 4. (A) Head, (B) velocity, and (C) solute mass flux changes with depth beneath Lisbon Valley at x = 31 km(see Fig. 2 for location of profile). The horizontal black lines denote the approximate position of the Paradox Formation beneath Lisbon Valley. Crystalline basement/laccolith permeability scenarios (1-3) are indicated by the black, red, and green solid lines. The dashed lines denote fault scenarios 4 and 5 from Table 4. The white dots and brackets indicate head observations within Lisbon Valley from Noyes (2019) and Thackston et al. (1981).

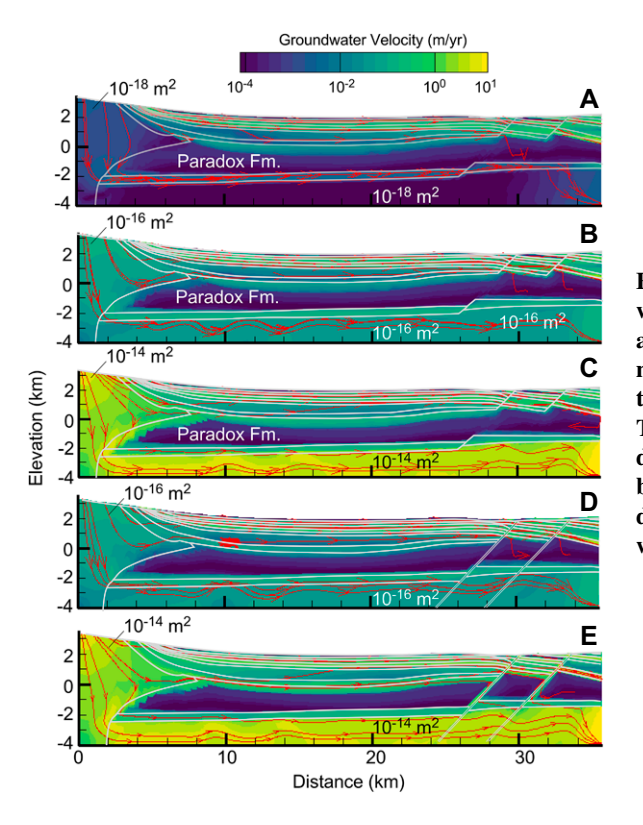


Figure 5. Computed ground-water velocity and streak lines across Lisbon Valley model domain. See Figure 1A for location of cross-section line A-A'. The translucent white lines denote formation and fault boundaries. The streak lines denote the direction of ground-water flow.

 10^{-18} m² to 10^{-16} m² and 10^{-14} m², respectively (Figs. 4B, 5B, and 5C). Groundwater streak lines (red arrows) in Figure 5 indicate that nearly all flow exits the model domain along the southern boundary. Groundwater flow directions are controlled, in large part, by permeability and the lat-

eral head gradient between the La Sal Mountains (\sim 2700 m) and the southern edge of the model domain (1830–1400 m). Groundwater velocities exceeded 1 m/yr within the permeable units of the upper aquifer system. The inclusion of anisotropic faults ($k_z > k_x$) did little to change the fluid

flux much within the upper aquifer system. For fault scenario 4 (Table 4), fluids moved into the GTO and Lisbon Valley faults within the upper aquifer system and migrated downward, terminating within the Paradox Formation (Fig. 5D) owing to the inward-directed hydraulic gradients within this underpressured formation (Corbet and Bethke, 1992). In fault scenario 5, some of the fluids entering the fault zone above the Paradox Formation migrated into the lower aquifer system (Fig. 5E).

Figure 6 presents computed salinity patterns for all modeled scenarios. The position of the mixing zone within the upper aquifer system was found to be sensitive to both crystalline basement permeability and the presence or absence of faults. Within the shallow units of the upper aquifer system, a topography-driven flow system extends down into the Cutler and Honaker Trail formations, maintaining low salinities. Salinities within the Cutler Formation increased along the flow path to the southeast as laccolith and crystalline basement permeability increased (Figs. 6A-6C). For high-permeability scenario 5, in which faults were added and horizontal permeability was lower (10^{-16} m^2) than that of the aguifers, the freshwater-saline water mixing zone rose into the Cutler Formation (Fig. 6E). The salinity in the lower aquifer system ranged between 100 ppt and 300 ppt, depending on the permeability of the crystalline basement. For the lowest crystalline basement permeability of 10⁻¹⁸ m2, the crystalline basement and lower aquifer system is dominated by high salinity (\sim 300 ppt;

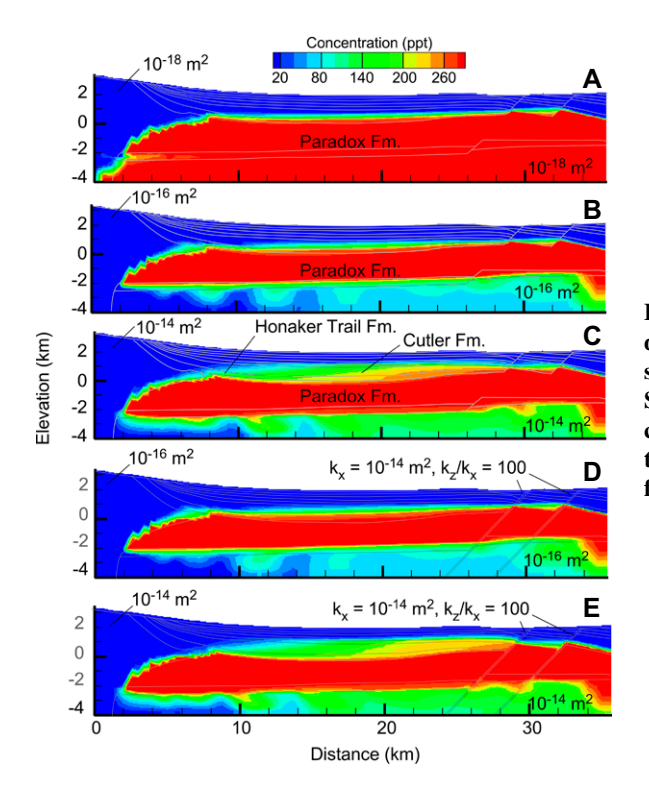


Figure 6. Computed modernday salinities from Pleistocene simulation along line A-A'. See Figure 1A for location of cross-section line A-A'. The translucent white lines denote formation and fault boundaries.

Figs. 6A and 7A). Simulations that considered higher permeabilities diluted salinity in the lower aquifer system and crystalline basement (Figs. 6B, 6C, and 7A). The intermediate permeability scenario is most consistent with measured salinities within the lower aquifer system across Lisbon Valley (Fig. 7A). The highest permeability scenario has the lowest computed salinity in other regions (e.g., x = 10 km; Fig. 6C). Transient haline-convection cells formed along the flow path within the crystalline basement (Fig. S1). Computed salinities are in reasonably good agreement with conditions observed for the intermediate- and high-permeability scenarios (blue dots, Fig. 7A; Kim et al., 2022a).

Computed mean groundwater ages are presented in Figure 8. Observed groundwater residence times within the upper aquifer system ranged from Pleistocene to Holocene (Fig. 7B). As crystalline basement permeability increased (Figs. 8A–8C), the volumes of relatively young meteoric fluids entering the Cutler and Honaker Trail formations rose. For scenario 4, faults with relatively low horizontal permeability had a barrier effect, increasing simulated groundwater age (Fig. 8D). Groundwater age within the Paradox Formation ranged between 4 Ma

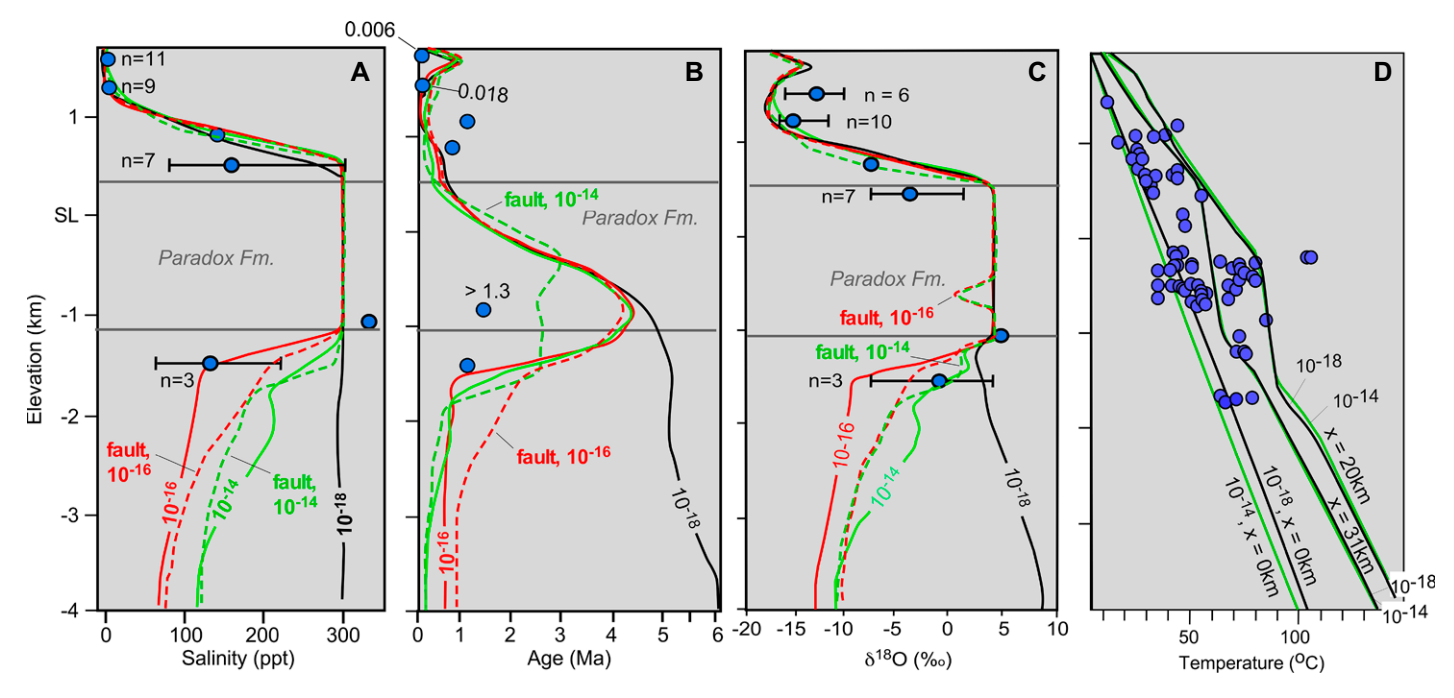


Figure 7. (A) Computed salinity, (B) mean groundwater residence time, and (C) $\delta^{18}O$ composition profiles within Lisbon Valley at x=31 km for all five modeled scenarios. Blue dots are observed average values. Whisker plot ends denote maximum and minimum observed values. Variable "n" denotes the number of observations. Crystalline basement/laccolith permeability scenarios (1–3) are indicated with the symbols 10^{-18} m² (solid black line), 10^{-16} m² (solid red line), and 10^{-14} m² (solid green line). Dashed lines denote fault scenarios 4 and 5 from Table 4. La Sal Laccolith and crystalline basement rocks were assigned a permeability of 10^{-16} m² (red dashed line) and 10^{-14} m² (green dashed line) in the fault scenarios. Blue dots with lines indicate mean, maximum, and minimum salinities. When maximum or minimum data were close to the mean or there was only one observation, a single dot was used. Most, but not all, of the observed salinity data were collected within Lisbon Valley. (D) Multiple temperature measurements (blue dots) were reported within individual Lisbon Valley wells.

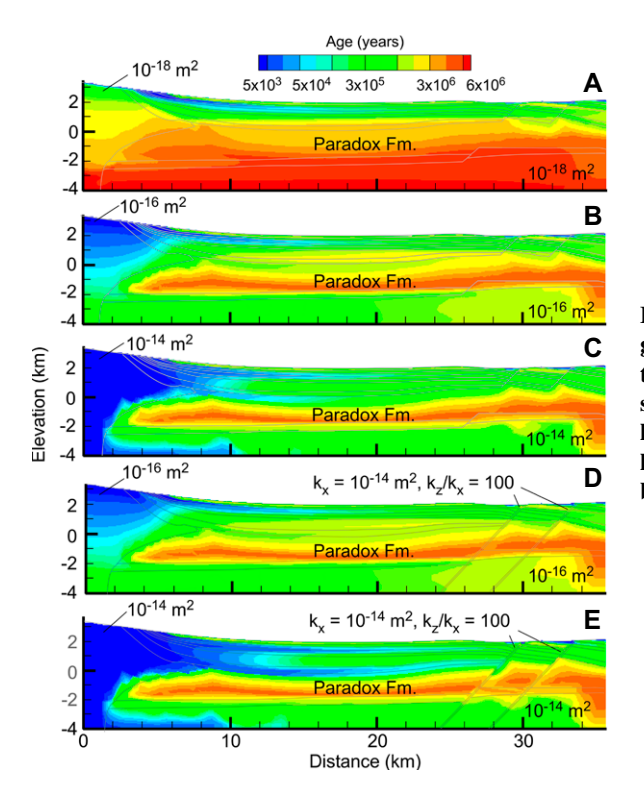


Figure 8. Computed modern-day groundwater ages from Pleistocene simulation along cross-section line A–A′ (see Fig. 1 for location). The translucent white lines denote formation and fault boundaries.

and 2 Ma. For the low-permeability crystalline basement scenarios (10⁻¹⁸ m²; Fig. 7B), groundwater age continued to increase in a nearly monotonic trend from the Paradox Formation to the bottom of the model domain. As crystalline basement permeability increased, relatively

younger groundwater was introduced beneath the Paradox Formation. Simulated ages for the intermediate- and high-permeability basement scenarios are consistent with ⁸¹Kr groundwater ages measured within Lisbon Valley (Fig. 7B; Kim et al., 2022b). Simulated groundwater ages

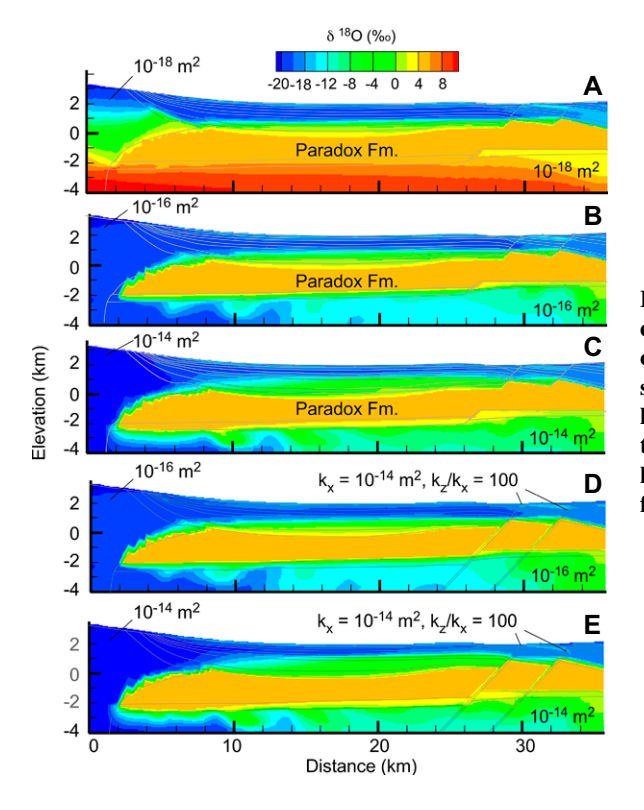


Figure 9. Computed modern-day groundwater $\delta^{18}O$ composition for Pleistocene simulations along cross-section line A-A' (see Fig. 1 for location). The translucent white lines denote formation and fault boundaries.

within the lower aquifer system are in reasonably good agreement with observed conditions for the intermediate- and high-permeability scenarios (Fig. 7B).

Simulated δ^{18} O values within the shallow aguifer system varied between about -13%to -18% (Fig. 9), which is consistent with the groundwater isotopic compositions measured by Noyes et al. (2021). The δ^{18} O values in the Paradox Formation were fixed at 5%o. Within the lower aquifer system and underlying crystalline basement, mixing between 18O-enriched fluids from the Paradox Formation and relatively δ18O-depleted meteoric recharge resulted in a net range of isotopic composition of between $\sim -8\%$ to +5% (Fig. 7C). Within the lower aquifer, simulated values of δ^{18} O for the highpermeability and fault scenarios came closest to matching the average δ^{18} O value reported by Kim et al. (2022a). For the low-permeability crystalline basement scenario (10⁻¹⁸ m²), the δ^{18} O values increased with depth to $\sim 9\%$ at the base of the model domain (Fig. 7C). Figure S1 compares temporal trends in δ^{18} O at the upper surface of the model near the top of the La Sal Mountains and Lisbon Valley within the Burro Canyon Formation, the lower aguifer system, and the crystalline basement (see white dots in Fig. 2A). For the high-permeability scenario, the effects of transient thermohaline convection cells on simulated $\delta^{18}O$ can be seen in the temporal trends in the isotopic composition of fluids within the crystalline basement; the transient thermohaline convection cells have a much shorter period than the climate forcing cells (Fig. S1C). In the Burro Canyon Formation (Fig. S1A), where flow variations are controlled by fluctuations in the water table, there are longer period and lower amplitude δ^{18} O variations than in the deeper aquifer (Fig. S1B). Long period, thermohaline convection developed in the intermediate permeability scenario within the lower aquifer system (Fig. S1B). Temporal variations in δ^{18} O within the crystalline basement (Fig. S1C) are observed for the high permeability scenario (10⁻¹⁴ m²).

Figure 10 presents computed temperatures for scenarios 1–5. Simulated temperatures are influenced by both convective heat transfer effects and the thermal conductivity contrast between the Paradox Formation and other units (Table 1). The absence of the Paradox Formation by the La Sal Laccolith created a complexity of simulated temperature patterns (Fig. 10A). The Paradox Formation is cut by the La Sal Laccolith between x=0–8 km created complexity in simulated conductive temperature patterns (Fig. 10A). The bulk thermal conductivity Paradox Formation (5.0 W-m/°C) is about twice that of the La Sal Laccolith unit. Increases in laccolith and crys-

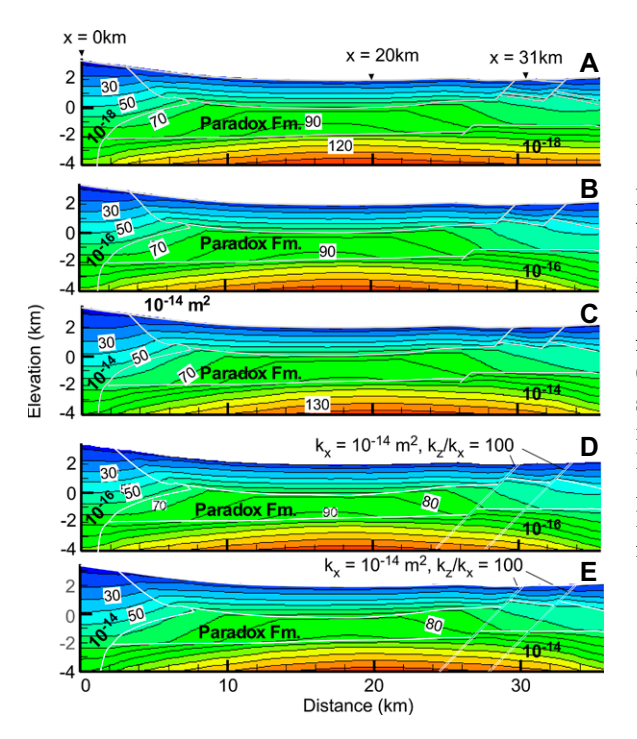


Figure 10. Computed temperatures (°C) along cross-section line A-A' for modeled scenarios 1-5. Locations of simulated temperature profiles extracted from model simulations at 0 km, 20 km, and 31 km presented in Figure 7D are shown in panel A. See Figure 1A for location of cross-section line A-A'. The translucent white lines denote formation and fault boundaries.

talline basement permeability resulted in convective cooling beneath the La Sal Mountains (note the change in position of the 50 °C isotherm between Figs. 10A-10C). Within Lisbon Valley, conductive heat transfer erased convective effects along the fault zones (Figs. 10D and 10E; Person et al., 2007). Figure 7D compares simulated temperature profiles at 0 km, 20 km, and 31 km along the model cross section to oil well temperature measurements collected during oil well shut-in tests conducted by Allis (2013). The broad range of temperatures below 2 km depth (43-104 °C) and changes in temperature gradients are largely due to the effects of thermal conductivity contrasts between the Paradox Formation and other units rather than convective effects (Fig. 7D). We are unaware of hot springs reported within the Paradox Basin. The change in slope of temperatures with depth occurs within the thermally conductive Paradox Formation.

DISCUSSION

This study demonstrates that laccoliths cutting sedimentary confining units created important pathways (hydrologic windows) for groundwater recharge into the lower aquifer system of the Paradox Basin and underlying crystalline basement rocks. Our hypothesis of deep groundwater circulation beneath the Colorado Plateau is not new. Crossey et al. (2009) used ³He/⁴He and ⁸⁷Sr/⁸⁶Sr data to argue that crystalline basement-hosted springs within the

great unconformity in the Grand Canyon region are associated with deep-flow system scavenging, mantle-derived 3He, and radiogenic Sr. Our findings that the upper aquifer system in the Paradox Basin is being recharged via the La Sal Mountain block are supported, in part, by the findings of Gardner et al. (2020). Interpreting the $\delta^{18}O$ data, these authors concluded that recharge to the Glenn Canyon Group, which includes the Navajo Sandstone, is being supplied via the fractured La Sal Laccolith rocks on the western side of the La Sal Mountains (see their fig. 10; Gardner et al., 2020). The observed salinity, groundwater residence times, and isotopic composition of pore fluids measured within the lower aguifer system by Kim et al. (2022a, 2022b) are consistent with modeled scenario results that assigned crystalline basement permeability in the intermediate-high range (10⁻¹⁶ m^2 to 10^{-14} m^2).

To test our hypothesis that the crystalline basement underlying the Paradox Basin is relatively permeable, we developed a simple one-dimensional analytical model of triggered seismicity. Ake et al. (2005) reported triggered seismicity after \sim 110 days of continuous brine injection into the Redwall Limestone at a rate of 1290 L/min within Paradox Valley. They indicated that the average formation pressure at the wellhead rose from \sim 42 MPa (hydrostatic) to 80 MPa ($\Delta P = 38$ MPa). The seismicity that was triggered occurred to \sim 5 km lateral distance and to a depth of up to \sim 1.2 km beneath the Redwall Limestone (Fig. 11A). To approxi-

mate the downward propagation of a pressure front beneath the Redwall Limestone, we used the following analytical model:

$$h(d,t) = h_o \operatorname{erfc}\left[\frac{d}{\sqrt{4D_h t}}\right],$$
 (1)

where h(d,t) is the computed, time-dependent anomalous head; d is depth below the injection horizon; erfc is the complementary error function; h_o is the value of elevated head in response to fluid injection (at d = 0, t > 0); t is time; S_s is specific storage (m^{-1}); and D_h is the hydraulic diffusivity $(K/S_s; m^2s^{-1})$, where K is hydraulic conductivity, which is a function of permeability ($K = k\rho_t g/\mu_t$; k is permeability, ρ_t is fluid density, μ_f is fluid viscosity, and g is gravity; ms⁻²). At time zero, heads/anomalous pressures are hydrostatic, i.e., 0 MPa, h(d,t=0). For t>0, the head at d = 0 was instantaneously increased to 38 MPa (3800 m). We report our results in equivalent anomalous pressures (MPa) rather than heads. Figure 11B presents earthquake foci as well as computed anomalous pressures after 110 days using basement permeabilities of 10^{-18} m^2 , 10^{-16} m^2 , and 10^{-14} m^2 . We assumed that S_s was 10⁻⁶ m⁻¹ within the crystalline basement. Pressure anomalies greater than 1 MPa occurring at a depth of 1 km are more than sufficient to trigger seismicity (Ge et al., 2009). The analytical solution results are most consistent with a crystalline basement permeability of 10^{-14} m².

Flow within the crystalline basement to depths of 7 km is certainly possible according to Ingebritsen and Manning (2010) and Manning and Ingebritsen (1999), who suggest that permeability at 10 km depth can be as high as 10^{-16} m² in geothermal and metamorphic environments. Precambrian basement rocks have relatively high permeabilities in the upper $1 \text{ km} (10^{-17} \text{ to } 10^{-14} \text{ m}^2)$ and lower permeabilities at greater depths (<10⁻¹⁸ m²), based on noble gas residence time tracers (Ferguson et al., 2023). In mountainous regions, topographically driven flow can drive meteoric fluids to depths of up to 5 km, based on stable water isotopes (McIntosh and Ferguson, 2021). The studies above primarily used geophysical and geochemical/isotopic datasets to arrive at their conclusions. Hydraulic tests conducted within deep boreholes also indicate relatively high crystalline basement permeability (Stober and Bucher, 2015a).

We computed the solute mass flux that exits Lisbon Valley (x=31 km) for all sensitivity study simulations (Fig. 4C). The solute mass flux within various aquifers in the upper aquifer system varied between $1.2 \times 10^4 \text{ kg/yr}$ to $4.6 \times 10^4 \text{ kg/yr}$. Solute mass flux migrating out of Lisbon

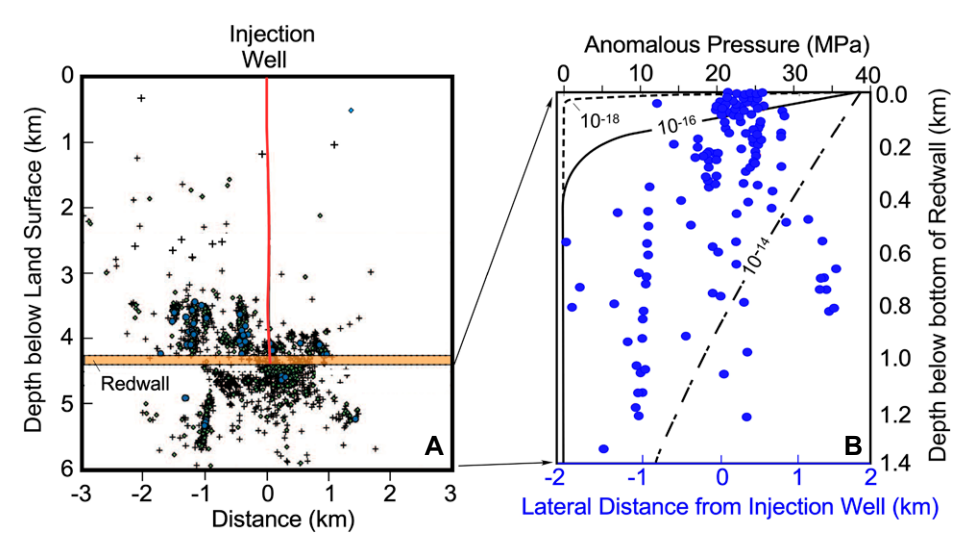


Figure 11. (A) Location of earthquake hypocenters of different magnitudes (+— \leq M1; diamond—M1–M2; blue dot— \geq M2) within Paradox Valley, Utah (after Ake et al., 2005). (B) Depth of hypocenters >M1 (blue circle) beneath the Redwall (also known as Leadville) Formation, as well as computed heads using error-function analytical solution for a basement permeability of 10^{-18} m² (dashed black line), 10^{-16} m² (solid black line), and 10^{-14} m² (long—short black dashed line) after 110 days. All analytic models assumed a specific storage (S_s) of 10^{-6} m $^{-1}$.

Valley beneath the Paradox Formation was $\sim 1.5 \times 10^2$ and 2×10^4 kg/yr for the low- and intermediate-permeability scenarios (10⁻¹⁸ m² to 10⁻¹⁶ m²), respectively. For the high basement permeability scenario (10⁻¹⁴ m²), the solute mass flux exiting Lisbon Valley was 8.5×10^4 kg/yr, similar to that exiting the upper aquifer system. Reitman et al. (2014), using a threedimensional mathematical model (SUTRA), estimated that the mass of salt discharging into the Colorado River from the Honaker Trail and Cutler formations within Gypsum Valley was 2.3×10^5 kg/yr. Where is this salt going? Within the upper aquifer system, the salt load is likely migrating toward the Dolores River to the north, which has an annual Cl flux of 1.3×10^8 kg/yr (Hite and Lohman, 1973). Within the crystalline basement, a component of the salt load may be migrating toward lowlands along the Colorado River. Crossey et al. (2009) noted that along the Colorado and Little Colorado rivers in the Grand Canyon, there is discharge of Na-Cl-rich fluids with total dissolved solids of up to 50 ppt. We hypothesize that some of these saline fluids may be derived from the Paradox Basin. The lower aquifer system potentiometric surface near Mexican Hat is lower than the elevation of the San Juan River (Fig. 1B), which suggests that groundwater flow is migrating southwestward toward the Grand Canyon.

In some settings, faults act as seals (Stober and Bucher, 2015b). This study did not find that faults were the locus of significant ground-

water transfer between the upper and lower aquifer systems. This is because the underpressured Paradox Formation was able to capture fluids migrating down faults beneath Lisbon Valley. Copper mineralization associated with fault zones within Lisbon Valley clearly indicates that faults focused vertical fluid flow in the geologic past (Jacobs and Kerr, 1965; Huntoon, 1986; Chan et al., 2000; Bailey et al., 2022). We argue that the topography-driven groundwater flow system is a relatively recent phenomena, perhaps only established in the past 2-5 m.y. (Murray et al., 2016; Kim et al., 2022b). During the Eocene, when 2 km of the Mancos Shale capped the Paradox Basin, thermohaline convection was likely the dominant mechanism driving fluid flow vertically along fault zones and may have been an important mechanism for ore mineralization.

Inspection of the time series of computed $\delta^{18}O$ values in Figure S1 suggests that the hydrologic system approached dynamic equilibrium conditions within the crystalline basement after 1 m.y. Within the Burro Canyon Formation (Fig. S1A), simulated temporal trends in $\delta^{18}O$ are out of phase and have a lower amplitude relative to the Pleistocene recharge signal (blue line in Fig. S1C; Loosli et al., 1998). Simulated temporal variations within the lower aquifer system and basement are controlled by the interplay between forced and thermohaline convection. It is worth noting that simulated thermohaline convection cells within the crystalline basement

are approximations of actual conditions. Haline convection cells are sensitive to grid discretization (Post and Kooi, 2003) as well as heterogeneity of spatial permeability (Gerdes et al., 1995) not represented in our simulations. The long simulation times required to reconstruct the paleo-hydrogeology of Lisbon Valley over the Pleistocene prevented us from considering additional grid refinement.

CONCLUSIONS

We used subsurface heat and mass transport models constrained by geochemical/isotopic data from Kim et al. (2022a, 2022b) to understand the hydrologic interactions between the La Sal Mountains and Paradox Basin near Lisbon Valley. An important component of La Sal Mountain recharge enters the upper aquifer system laterally through the mountain block. A fresh-saline water mixing zone develops within the Honaker Trail and Cutler formations within the upper aquifer system. The anisotropic faults $(k_z > k_x)$ in our model acted mainly as a barrier to lateral flow. Fluid-impelling mechanisms within the lower aquifer system and underlying crystalline basement include both topographyand density-driven flow (haline convection). Underpressures form within the low-permeability Paradox Formation due to erosion and sediment decompaction.

Importantly, we found that the La Sal Mountains act as a hydrologic window into the lower aquifer system and underlying crystalline basement. For scenarios where the crystalline basement was relatively permeable (10⁻¹⁶ m² to 10^{-14} m²), meteoric fluids mixed with brines of the Paradox Formation. Models that included a permeable crystalline basement were largely in agreement with isotopic tracers and salinity data reported by Kim et al. (2022a, 2022b). The presence of faults did not significantly modify fluid exchange between the upper and lower aquifer systems. This was due to underpressuring within the Paradox Formation (Fig. 1D). We hypothesize that the downward hydraulic gradient observed beneath Lisbon Valley is the result of a long-distance hydrologic connection to crystalline basement rocks that outcrop along the Colorado River at lower elevations perhaps as far away as the Grand Canyon. Meteoric recharge through hydrologic windows may have reintroduced microbial communities into previously sterilized sediments at the bottom of the Paradox Basin (McIntosh et al., 2023).

This study highlights the importance of groundwater circulation through the relatively permeable crystalline basement and its interactions with overlying/adjacent sedimentary basin

units. Sedimentary basins should no longer be thought of as closed hydrologic systems. They have porous lower boundaries through which solutes, heat, and microorganisms (Crossey et al., 2016; McIntosh et al., 2023) are transported. Our findings may also have implications for the involvement of crystalline basement in the formation of Mississippi Valley-type ore deposits (Wilkinson, 2010).

ACKNOWLEDGMENTS

We thank Steve Ingebritsen for his assistance in revising this manuscript. Support from the W.M. Keck Foundation (grant no. 989941) and the National Science Foundation (National Science Foundation Frontier Research in Earth Sciences grant no. 1925974 and Division of Earth Sciences grant no. 1830172) is gratefully acknowledged. Support to Jennifer McIntosh under National Science Foundation Frontier Research in Earth Sciences Subsurface Microbe-Rock-Fluid Systems grant no. 2120733 is gratefully acknowledged.

REFERENCES CITED

- Ake, J., Mahrer, K., O'Connell, D., and Block, L., 2005, Deep-injection and closely monitored induced seismicity at Paradox Valley, Colorado: Bulletin of the Seismological Society of America, v. 95, no. 2, p. 664–683, https://doi.org/10.1785/0120040072.
- Allen, B.D., 2005, Ice age lakes in New Mexico: New Mexico's ice ages: New Mexico Museum of Natural History and Science Bulletin, v. 28, p. 107–113.
- Allis, R., 2013, Utah NGDS drill-stem test data wildcat wells in western Utah: Utah Geological Survey.
- Aquilina, L., de Dreuzy, J.R., Bour, O., and Davy, P., 2004, Porosity and fluid velocities in the upper continental crust (2 to 4 km) inferred from injection tests at the Soultz-sous-Forêts geothermal site: Geochimica et Cosmochimica Acta, v. 68, no. 11, p. 2405–2415, https:// doi.org/10.1016/j.gca.2003.08.023.
- Bailey, L.R., Kirk, J., Hemming, S.R., Krantz, R.W., and Reiners, P.W., 2022, Eocene fault-controlled fluid flow and mineralization in the Paradox Basin, United States: Geology, v. 50, no. 3, p. 326–330, https://doi.org/10 .1130/G49466.1.
- Baker, A.A., Dane, C.H., and Reeside, J.B., Jr., 1933, Paradox Formation of eastern Utah and western Colorado: American Association of Petroleum Geologists Bulletin, v. 17, no. 8, p. 963–980.
- Barbeau, D.L., 2003, Å flexural model for the Paradox Basin, implications for the tectonics of the Ancestral Rocky Mountains: Basin Research, v. 15, no. 1, p. 97–115, https://doi.org/10.1046/j.1365-2117.2003.00194.x.
- Barroll, M.W., and Reiter, M., 1990, Analysis of the Socorro hydrogeothermal system: Central New Mexico: Journal of Geophysical Research: Solid Earth, v. 95, no. B13, p. 21,949–21,963, https://doi.org/10.1029 /JB095iB13p21949.
- Beauheim, R.L., and Roberts, R.M., 2002, Hydrology and hydraulic properties of a bedded evaporite formation: Journal of Hydrology, v. 259, no. 1–4, p. 66–88, https://doi.org/10.1016/S0022-1694(01)00586-8.
- Belitz, K., and Bredehoeft, J.D., 1988, Hydrodynamics of Denver Basin: Explanation of subnormal fluid pressures: American Association of Petroleum Geologists Bulletin, v. 72, no. 22, p. 1334–1359.
- Benson, L.V., 1988, Preliminary paleolimnologic data for the Walker Lake subbasin, California and Nevada: U.S. Geological Survey Water Resources Investigations Report 87-4258.
- Bowman, J.R., Willett, S.D., and Cook, S.J., 1994, Oxygen isotopic transport and exchange during fluid flow: Onedimensional models and applications: American Journal of Science, v. 294, no. 1, https://doi.org/10.2475/ajs.294.1.1.

- Bredehoeft, J.D., Neuzil, C.E., and Milly, P.C.D., 1983, Regional flow in the Dakota Aquifer: A study of the role of confining layers: U.S. Geological Survey Water Supply Paper 2237, 45 p.
- Bucher, K., Zhang, L., and Stober, I., 2009, A hot spring in granite of the Western Tianshan, China: Applied Geochemistry, v. 24, p. 402–410, https://doi.org/10.1016/j .apgeochem.2008.12.021.
- Cappa, J.A., and Rice, D.D., 1995, Carbon dioxide in Mississippian rocks of the Paradox Basin and adjacent areas, Colorado, Utah, New Mexico, and Arizona: U.S. Geological Survey Bulletin 2000-H.
- Chan, M.A., Parry, W.T., and Bowman, J.R., 2000, Diagenetic hematite and manganese oxides and fault-related fluid flow in Jurassic sandstones, southeastern Utah: The American Association of Petroleum Geologists Bulletin, v. 84, no. 9, p. 1281–1310.
- Chan, M.A., Parry, W.T., Petersen, E.U., and Hall, C.M., 2001, ⁴⁰Ar/³⁹Ar age and chemistry of manganese mineralization in the Moab and Lisbon fault systems, southeastern Utah: Geology, v. 29, no. 4, p. 331–334, https:// doi.org/10.1130/0091-7613(2001)029<0331:AAA ACO>2.0.CO;2.
- Chidsey, T.C., Jr., Eby, D.E., and Wray, L.L., 2003, Porosity/ permeability cross-plots: Cherokee and Bug Fields, San Juan County, Utah, and Little Ute and Sleeping Fields, San Montezuma County, Colorado: Utah Geological Survey.
- Clem, K.M., and Brown, K.W., 1984, Petroleum resources of the Paradox Basin: Utah Geological Survey, v. 119.
- Cole, R.D., Moore, G.E., Trevena, A.S., Armin, R.A., and Morton, M.P., 1996, Lithofacies definition in Cutler and Honaker Trail formations, northeastern Paradox Basin, by sedimentologic observations and spectral gammaray data: American Association of Petroleum Geologists Archives Datapages.
- Condon, S.M., 1997, Geology of the Pennsylvanian and Permian Cutler Group and Permian Kaibab Limestone in the Paradox Basin, southeastern Utah and southwestern Colorado: U.S. Geological Survey Bulletin 2000-P.
- Corbet, T.F., and Bethke, C.M., 1992, Disequilibrium fluid pressures and groundwater flow in the western Canada sedimentary basin: Journal of Geophysical Research: Solid Earth, v. 97, no. B5, p. 7203–7217, https://doi.org/10.1029/91JB02993.
- Crossey, L.J., Karlstrom, K.E., Springer, A.E., Newell, D., Hilton, D.R., and Fischer, T., 2009, Degassing of mantle-derived CO₂ and He from springs in the southern Colorado Plateau region—Neotectonic connections and implications for groundwater systems: Geological Society of America Bulletin, v. 121, no. 7–8, p. 1034–1053, https://doi.org/10.1130/B26394.1.
- Crossey, L.J., Karlstrom, K.E., Schmandt, B., Crow, R.R., Colman, D.R., Cron, B., Takacs-Vesbach, C.D., Dahm, C.N., Northup, D.E., Hilton, D.R., and Ricketts, J.W., 2016, Continental smokers couple mantle degassing and distinctive microbiology within continents: Earth and Planetary Science Letters, v. 435, p. 22–30, https:// doi.org/10.1016/j.epsl.2015.11.039
- Ferguson, G., McIntosh, J., Warr, O., and Sherwood Lollar, B., 2023, The low permeability of the Earth's Precambrian crust: Communications Earth & Environment, v. 4, no. 1, 323, https://doi.org/10.1038/s43247-023-00968-2.
- Freethey, G.W., and Cordy, G.E., 1991, Geohydrology of Mesozoic rocks in the Upper Colorado River Basin in Arizona, Colorado, New Mexico, Utah, and Wyoming, excluding the San Juan Basin: U.S. Geological Survey Professional Paper 1411-C.
- Frisbee, M.D., Tolley, D.G., and Wilson, J.L., 2017, Field estimates of groundwater circulation depths in two mountainous watersheds in the western US and the effect of deep circulation on solute concentrations in streamflow: Water Resources Research, v. 53, no. 4, p. 2693–2715, https://doi.org/10.1002/2016WR019553.
- Gardner, P.M., Nelson, N.C., Heilweil, V.M., Solder, J.E., and Solomon, D.K., 2020, Rethinking a groundwater flow system using a multiple-tracer geochemical approach: A case study in Moab-Spanish Valley, Utah: Journal of Hydrology, v. 590, https://doi.org/10.1016 /j.jhydrol.2020.125512.
- Ge, S., Liu, M., Lu, N., Godt, J.W., and Luo, G., 2009, Did the Zipingpu Reservoir trigger the 2008 Wenchuan

- earthquake?: Geophysical Research Letters, v. 36, no. 20, https://doi.org/10.1029/2009GL040349.
- Gerdes, M., Baumgartner, L., and Person, M., 1995, Permeability heterogeneity in metamorphic rocks: Implications from stochastic modeling: Geology, v. 23, p. 945–948, https://doi.org/10.1130/0091-7613(1995)023<0945:SPMOFF>2.3.CO;2.
- Goldhammer, R.K., Oswald, E.J., Dunn, P.A., Franseen, E.K., and Watney, W.L., 1991, Hierarchy of stratigraphic forcing: Example from middle Pennsylvanian shelf carbonates of the Paradox Basin: Kansas Geological Survey Bulletin, v. 233, p. 361–413.
- Goode, D.J., 1996, Direct simulation of groundwater age: Water Resources Research, v. 32, no. 2, p. 289–296, https://doi.org/10.1029/95WR03401.
- Gregory, R.T., Criss, R.E., and Taylor, H.P., Jr., 1989, Oxygen isotope exchange kinetics of mineral pairs in closed and open systems: Applications to problems of hydrothermal alteration of igneous rocks and Precambrian iron formations: Chemical Geology, v. 75, no. 1–2, p. 1–42, https://doi.org/10.1016/0009-2541(89)90019-3.
- Gutierrez, M., Katsuki, D., and Tutuncu, A., 2015, Determination of the continuous stress-dependent permeability, compressibility and poroelasticity of shale: Marine and Petroleum Geology, v. 68, p. 614–628, https://doi.org/10.1016/j.marpetgeo.2014.12.002.
- Hanshaw, B.B., and Hill, G.A., 1969, Geochemistry and hydrodynamics of the Paradox Basin region, Utah, Colorado and New Mexico: Chemical Geology, v. 4, no. 1–2, p. 263–294, https://doi.org/10.1016/0009 -2541(69)90050-3.
- Heath, J.E., Dewers, T., Chidsey, T.C., Carney, S.M., and Bereskin, S.R., 2017, The Gothic Shale of the Pennsylvanian Paradox Formation, Greater Aneth Field (Aneth Unit), Southeastern Utah, USA: Seal for Hydrocarbons and Carbon Dioxide Storage: Albuquerque, New Mexico, Sandia National Lab, no. SAND2017-4825R.
- Hite, R.J., and Lohman, S.W., 1973, Geologic appraisal of Paradox Basin salt deposits for water emplacement: U.S. Geological Survey Open-File Report 73-114.
- Hunt, C.B., and Waters, A.C., 1958, Structural and igneous geology of the La Sal Mountains, Utah: U.S. Geological Survey Professional Paper 294-I, p. 305–364.
- Huntoon, P.W., 1986, Incredible tale of Texas gulf well 7 and fracture permeability, Paradox Basin, Utah: Groundwater, v. 24, no. 5, p. 643–653, https://doi.org/10.1111/j.1745-6584.1986.tb03713.x.
- Ingebritsen, S.E., and Manning, C.E., 2010, Permeability of the continental crust: Dynamic variations inferred from seismicity and metamorphism: Geofluids, v. 10, no. 1–2, p. 193–205.
- Jacobs, M.B., and Kerr, P.F., 1965, Hydrothermal alteration along the Lisbon Valley fault zone, San Juan County, Utah: Geological Society of America Bulletin, v. 76, no. 4, p. 423–440, https://doi.org/10.1130/0016-7606(1965)76[423:HAATLV]2.0.CO;2.
- Kim, J.H., Bailey, L., Noyes, C., Tyne, R.L., Ballentine, C.J., Person, M., Ma, L., Barton, M., Barton, I., Reiners, P.W., Ferguson, G., and McIntosh, J., 2022a, Hydrogeochemical evolution of formation waters responsible for sandstone bleaching and ore mineralization in the Paradox Basin, Colorado Plateau, USA: Geological Society of America Bulletin, v. 134, no. 9–10, p. 2589–2610, https://doi.org/10.1130/B36078.1.
- Kim, J.H., Ferguson, G., Person, M., Jiang, W., Lu, Z.T., Ritterbusch, F., Yang, G.M., Tyne, R., Bailey, L., Ballentine, C., Reiners, P., and McIntosh, J., 2022b, Krypton-81 dating constrains timing of deep groundwater flow activation: Geophysical Research Letters, v. 49, no. 11, https://doi.org/10.1029/2021GI.097618.
- Kirby, S.M., 2008, Geologic and hydrologic characterization of the Dakota-Burro Canyon aquifer near Blanding, San Juan County, Utah: Utah Geological Survey Special Study 123.
- Lollar, G.S., Warr, O., Telling, J., Osburn, M.R., and Lollar, B.S., 2019, 'Follow the water': Hydrogeochemical constraints on microbial investigations 2.4 km below surface at the Kidd Creek deep fluid and deep life observatory: Geomicrobiology Journal, v. 36, no. 10, p. 859–872, https://doi.org/10.1080/01490451.2019.1641770.
- Loosli, H.H., Lehmann, B., Aeschbach-Hertig, W., Kipfer, R., Edmunds, W.M., Eichinger, L., Rozanski, K., Stute,

- M., and Vaikmäe, R., 1998, Tools used to study paleoclimate help in water management: Eos (Transactions, American Geophysical Union), v. 79, no. 47, p. 576–582, https://doi.org/10.1029/98EO00422.
- Lopes, T.J., and Hoffmann, J.P., 1997, Geochemical analyses of ground-water ages, recharge rates, and hydraulic conductivity of the N aquifer, Black Mesa area, Arizona: U.S. Geological Survey Water Resources Investigations Report 96-4190.
- Mailloux, B.J., Person, M., Kelley, S., Dunbar, N., Cather, S., Strayer, L., and Hudleston, P., 1999, Tectonic controls on the hydrogeology of the Rio Grande Rift, New Mexico: Water Resources Research, v. 35, no. 9, p. 2641– 2659, https://doi.org/10.1029/1999WR900110.
- Manning, C.E., and Ingebritsen, S.E., 1999, Permeability of the continental crust: The implications of geothermal data and metamorphic systems: Reviews of Geophysics, v. 37, p. 127–150, https://doi.org/10.1029 /1998RG900002.
- McIntosh, J., Kim, J.H., Bailey, L., Osburn, M., Drake, H., Martini, A., Reiners, P., Stevenson, B., and Ferguson, G., 2023, Burial and denudation alter microbial life at the bottom of the hypo-critical zone: Geochemistry, Geophysics, Geosystems, v. 24, no. 6, https://doi.org /10.1029/2022GC010831.
- McIntosh, J.C., and Ferguson, G., 2021, Deep meteoric water circulation in Earth's crust: Geophysical Research Letters, v. 48, no. 5, https://doi.org/10.1029 /2020GL090461.
- McKee, E.D., and Gutschick, R.C., 1969, History of the Redwall Limestone of Northern Arizona: Geological Society of America Memoir 114, 726 p., https://doi.org /10.1130/MEM114-p1.
- Menking, K.M., Anderson, R.Y., Shafike, N.G., Syed, K.H., and Allen, B.D., 2004, Wetter or colder during the Last Glacial Maximum?: Revisiting the pluvial lake question in southwestern North America: Quaternary Research, v. 62, no. 3, p. 280–288, https://doi.org/10.1016/j.yqres .2004.07.005.
- Meyers, Z.P., Frisbee, M.D., Rademacher, L.K., and Stewart-Maddox, N.S., 2021, Old groundwater buffers the effects of a major drought in groundwater-dependent ecosystems of the eastern Sierra Nevada (CA): Environmental Research Letters, v. 16, no. 4, 044044, https:// doi.org/10.1088/1748-9326/abde5f.
- Murray, K.E., Reiners, P.W., and Thomson, S.N., 2016, Rapid Pliocene–Pleistocene erosion of the central Colorado Plateau documented by apatite thermochronology from the Henry Mountains: Geology, v. 44, no. 6, p. 483– 486, https://doi.org/10.1130/G37733.1.
- Neuzil, C.E., 1994, How permeable are clays and shales?: Water Resources Research, v. 30, no. 2, p. 145–150, https://doi.org/10.1029/93WR02930.
- Noyes, C., Kim, J., Person, M., Ma, L., Ferguson, G., and McIntosh, J.C., 2021, A geochemical and isotopic assessment of hydraulic connectivity of a stacked aquifer system in the Lisbon Valley, Utah (USA), and critical evaluation of environmental tracers: Hydrogeology Journal, v. 29, p. 1905–1923, https://doi.org/10.1007 /s10040-021-02361-9.
- Noyes, C.E., 2019, Geochemical and isotopic assessment of regional groundwater flow and aquifer connectivity in the Lisbon Valley, Utah [Ph.D. dissertation]: Tucson, Arizona, The University of Arizona, 95 p.
- Nuccio, V.F., and Condon, S.M., 1996, Burial and thermal history of the Paradox Basin, Utah and Colorado, and petroleum potential of the middle Pennsylvanian Paradox Formation: U.S. Geological Survey Bulletin 2000-O, 47 p.

- Paces, J.B., Palmer, M.V., Palmer, A.N., Long, A.J., and Emmons, M.P., 2020, 300,000 yr history of water-table fluctuations at Wind Cave, South Dakota, USA—Scale, timing, and groundwater mixing in the Madison Aquifer: Geological Society of America Bulletin, v. 132, no. 7–8, p. 1447–1468, https://doi.org/10.1130/B35312.1.
- Pepin, J.D., Person, M., Phillips, F., Kelley, S., Timmons, S., Owens, L., Witcher, J., and Gable, C.W., 2012, Deep fluid circulation within crystalline basement rocks and the role of hydrologic windows in the formation of the Truth or Consequences, New Mexico low-temperature geothermal system, in Gleeson, T., and Ingebritse, S.E., eds., Crustal Permeability: John Wiley & Sons, p. 155–173, https://onlinelibrary.wiley.com/doi/10.1002/9781119166573.ch14.
- Person, M., Mulch, A., Teyssier, C., and Gao, Y., 2007, Isotope transport and exchange within metamorphic core complexes: American Journal of Science, v. 307, no. 3, p. 555–589, https://doi.org/10.2475/03.2007.01.
- Phillips, F.M., Peeters, L.A., Tansey, M.K., and Davis, S.N., 1986, Paleoclimatic inferences from an isotopic investigation of groundwater in the central San Juan Basin, New Mexico: Quaternary Research, v. 26, no. 2, p. 179– 193, https://doi.org/10.1016/0033-5894(86)90103-1.
- Post, V., Kooi, H., and Simmons, C., 2007, Using hydraulic head measurements in variable-density ground water flow analyses: Groundwater, v. 45, no. 6, p. 664–671, https://doi.org/10.1111/j.1745-6584.2007.00339.x.
- Post, V.E.A., and Kooi, H., 2003, Rates of salinization by free convection in high-permeability sediments: Insights from numerical modeling and application to the Dutch coastal area: Hydrogeology Journal, v. 11, p. 549–559, https://doi.org/10.1007/s10040-003-0271-7.
- Putnam, A.E., and Broecker, W.S., 2017, Human-induced changes in the distribution of rainfall: Science Advances, v. 3, no. 5, https://doi.org/10.1126/sciadv.1600871.
- Rasmussen, L., and Rasmussen, D.L., 2009, Burial History Analysis of the Pennsylvanian Petroleum System in the Deep Paradox Basin Fold and Fault Belt, Colorado and Utah: Rocky Mountain Association of Geologists, p. 24–94.
- Reheis, M.C., Adams, K.D., Oviatt, C.G., and Bacon, S.N., 2014, Pluvial lakes in the Great Basin of the western United States—A view from the outcrop: Quaternary Science Reviews, v. 97, p. 33–57, https://doi.org/10 .1016/j.quascirev.2014.04.012.
- Reitman, N.G., Ge, S., and Mueller, K., 2014, Groundwater flow and its effect on salt dissolution in Gypsum Canyon watershed, Paradox Basin, southeast Utah, USA: Hydrogeology Journal, v. 22, no. 6, p. 1403–1419, https://doi.org/10.1007/s10040-014-1126-0.
- Richmond, G.M., 1972, Appraisal of the future climate of the Holocene in the Rocky Mountains: Quaternary Research, v. 2, no. 3, p. 315–322, https://doi.org/10.1016 /0033-5894(72)90051-8.
- Shipton, Z.K., Evans, J.P., Kirschner, D., Kolesar, P.T., Williams, A.P., and Heath, J., 2004, Analysis of CO2 leakage through 'low-permeability' faults from natural reservoirs in the Colorado Plateau, east-central Utah, in Baines, S.J., and Worden, R.H., eds., Geological Storage of Carbon Dioxide: Geological Society, London, Special Publication 233, p. 43–58, https://doi.org/10 .1144/GSL.SP.2004.233.01.05.
- Simmons, G.C., 1957, Contact of Burro Canyon Formation with Dakota Sandstone, Slick Rock District, Colorado, and correlation of Burro Canyon Formation: AAPG Bulletin, v. 41, no. 11, p. 2519–2529.
- Stober, I., 1996, Researchers study conductivity of crystalline rock in proposed radioactive waste site: Eos (Transactions, American Geophysical Union), v. 77, no. 10, p. 93–94.

- Stober, I., and Bucher, K., 2004, Fluid sinks within the Earth's crust: Geofluids, v. 4, p. 143–151, https://doi. org/10.1111/j.1468-8115.2004.00078.x.
- Stober, I., and Bucher, K., 2007, Hydraulic properties of the crystalline basement: Hydrogeology Journal, v. 15, p. 213–224, https://doi.org/10.1007/s10040-006 -0094-4.
- Stober, I., and Bucher, K., 2015a, Hydraulic and hydrochemical properties of deep sedimentary aquifers of the Upper Rhine Graben, Europe: Geofluids, v. 15, p. 464–482, https://doi.org/10.1111/gfl.12122.
- Stober, I., and Bucher, K., 2015b, Hydraulic conductivity of fractured upper crust: Insights from hydraulic tests in boreholes and fluid-rock interaction in crystalline basement rocks: Geofluids, v. 15, p. 161–178, https://doi.org/ /10.1111/gfl.12104.
- Stober, I., Richter, A., Brost, E., and Bucher, K., 1999, The Ohlsbach Plume: Natural release of deep saline water from the crystalline basement of the Black Forest: Hydrogeology Journal, v. 7, no. 3, p. 273–283, https://doi .org/10.1007/s100400050201.
- Stober, I., Zhong, J., Zhang, L., and Bucher, K., 2016, Deep hydrothermal fluid–rock interaction: The thermal springs of Da Qaidam, China: Geofluids, v. 16, p. 711– 728, https://doi.org/10.1111/gfl.12190.
- Taucare, M., Viguier, B., Daniele, L., Heuser, G., Arancibia, G., and Leonardi, V., 2020, Connectivity of fractures and groundwater flows analyses into the Western Andean Front by means of a topological approach (Aconcagua Basin, Central Chile): Hydrogeology Journal, https://doi.org/10.1007/s10040-02200-3.
- Thackston, J.W., McCulley, B.L., and Preslo, L.M., 1981, Ground-water circulation in the western Paradox Basin, Utah, in Proceedings, 1981 Field Conference: Rocky Mountain Association of Geologists, p. 201–225.
- Tyne, R.L., Barry, P.H., Cheng, A., Hillegonds, D.J., Kim, J.H., McIntosh, J.C., and Ballentine, C.J., 2022, Basin architecture controls on the chemical evolution and ⁴He distribution of groundwater in the Paradox Basin: Earth and Planetary Science Letters, v. 589, https://doi.org/10.1016/j.epsl.2022.117580.
- Wilkinson, J.J., 2010, A review of fluid inclusion constraints on mineralization in the Irish ore field and implications for the genesis of sediment-hosted Zn-Pb deposits: Economic Geology, v. 105, no. 2, p. 417–442, https://doi .org/10.2113/gsecongeo.105.2.417.
- Woodward-Clyde Consultants, 1982, Geologic characterization report for the Paradox Basin study region, Utah study areas: Columbus, Ohio, Woodward-Clyde Consultants.
- Zhang, Y., Person, M., Rupp, J., Ellett, K., Celia, M.A., Gable, C.W., Bowen, B., Evans, J., Bandilla, K., Mozley, P., and Dewers, T., 2013, Hydrogeologic controls on induced seismicity in crystalline basement rocks due to fluid injection into basal reservoirs: Groundwater, v. 51, no. 4, p. 525–538, https://doi.org/10.1111/gwat 12071.
- Zhu, C., Winterle, J.R., and Love, E.I., 2003, Late Pleistocene and Holocene groundwater recharge from the chloride mass balance method and chlorine-36 data: Water Resources Research, v. 39, no. 7, https://doi.org/10.1029/2003WR001987.

SCIENCE EDITOR: WENJIAO XIAO ASSOCIATE EDITOR: DAVID MACDONALD

Manuscript Received 2 April 2023 Revised Manuscript Received 19 September 2023 Manuscript Accepted 30 October 2023